JOURNAL OF SPACECRAFT AND ROCKETS
Vol. 44, No. 3, May–June 2007

Modeling of Triangular Lattice Space Structures with Curved Battens

Tzikang Chen* and John T. Wang†
NASA Langley Research Center, Hampton, Virginia 23681

DOI: 10.2514/1.22628

Lightweight triangular lattice beams containing longerons, curved battens, and diagonals have been selected for many space structure applications, such as the supporting booms of future solar sails. The curved battens provide the flexibility needed for the booms to be twisted (coiled) and compressed to a small packing volume for reducing the launch cost. An integrated modeling technique for the analysis of triangular lattice beams with curved battens is presented. This modeling technique is used to simulate the assembly process of a lattice beam and to account for the assembly induced prestresses as well as the curvature of the battens in the subsequent loading response analysis. A key element of this integrated modeling technique is the implementation of a nonlinear cable-pulley element in a general-purpose finite element code. Finite element models representing different assembled-structure configurations were developed for investigating the effects of design variations on the load-carrying capabilities. The results indicate that both the curvature of the battens and the prestress state need to be modeled correctly for an accurate prediction of structural response. It is also shown that the loading capabilities of lattice beams can be significantly reduced if the cable diagonals are not constrained and are allowed to slide freely at the batten-longeron joints.

Introduction

LIGHTWEIGHT lattice structures are being considered for many future space structure applications such as booms for antennas, telescopes, and solar sails. For example, the triangular lattice beam column [1,2] shown in Fig. 1 is being developed under the support of the NASA In-Space Propulsion Technologies Program for solar-sail masts. This type of lattice structure contains very flexible components such as longerons, battens, and diagonals. The longerons are the main load-carrying members. The battens are used to keep the longerons in position and maintain the cross-sectional shape. The diagonals are tension cables that are used to provide shear stiffness. A useful attribute of this type of lattice structure is that it can be twisted and compressed (coiled) to a very small-volume package, which is important in reducing the launch cost. In addition, the stored elastic strain energy can be used to deploy the structure in space.

For a lattice beam that can be twisted and compressed into a small-volume package before deployment, the battens are designed to be curved [1,2], as shown in Fig. 1. During the manufacturing assembly, the initially straight battens are bent elastically into a curved form. To maintain the batten curvature, an axial compression force is induced in the battens by tensioning the diagonals. Therefore, the assembled lattice beam is in a prestressed state. To accurately determine the assembly induced prestresses and the shapes of the curved battens, techniques that can simulate the assembly process need to be developed.

Triangular lattice beams have been analyzed by many researchers [3–6]. For example, analytical solutions that address the effects of local and global longeron imperfections on the axial compressive strength of lattice columns have been presented by Crawford and Hedgepeth [3], Mikulas [4], and Crawford and Benton [5]. The finite element (FE) method and the equivalent-continuum method have also been widely used for analyzing this type of structure, as summarized by Noor [6]. However, in [3–6], the assembly induced prestresses were not included and the battens were designed as straight beams. After careful review of the literature, it appears that there are no published analysis results related to simulating the assembly process to account for the prestress state in the assembled structure. In addition no analyses have been found that model lattice beams with curved battens.

The objectives of this paper are to develop modeling techniques that can simulate adequately the assembly process of lattice beams, and to evaluate the effects of batten curvatures, assembly induced prestresses, and diagonal constraints on the loading responses of the assembled lattice beams. The loading responses such as load-carrying capability, deformed shape, and stiffness were also investigated. In the assembly, continuous cable diagonals were used that can slip through batten-longeron joints to adjacent bays. To simulate the cable diagonal sliding freely at a batten-diagonal joint in the assembly process, a cable-pulley element developed in [7] was implemented in the ABAQUS [8] finite element code. After the assembly, the cable diagonals were constrained at every batten-longeron joint and became discrete. The tension forces in the diagonals, the compression forces in the battens, and the curvatures of the battens in the assembled configuration were determined by performing geometrically nonlinear analyses that simulate the assembly process.

The paper is organized as follows. First, an assembly process of a lattice beam is proposed and a procedure for simulating the assembly process is presented, using a geometrically nonlinear analysis procedure of the ABAQUS finite element code. Next, three types of finite element models associated with the assembled lattice beam are described, using different modeling approaches to study the effects of the batten curvatures, prestresses, and cable-diagonal constraints. Then, the predicted loading responses are presented for these models being cantilevered at one end and subjected to a transverse tip load at the other end. Finally, the effects of using different modeling approaches on the lattice-beam loading response predictions are discussed.

Assembly Process for a Lattice Beam

An assembly process is proposed in this section for the lattice beam with curved battens shown in Fig. 2. Although this process may

Presented as Paper 1967 at the 46th AIAA/ASME/ASCE/AHS/ASC Structures, Structural Dynamics, and Materials Conference, Austin, TX, 18–21 April 2005; received 27 January 2006; revision received 28 November 2006; accepted for publication 24 October 2006.

*Mechanical Engineer, Vehicle Technology Directorate, Army Research Laboratory, Computational Structures and Materials Branch, MS 188E.

†Aerospace Engineer, Computational Structures and Materials Branch, MS 188E. Senior Member AIAA.

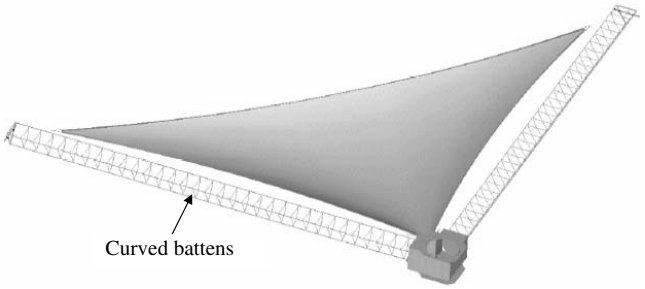

Fig. 1 Depiction of a 10-m solar-sail quadrant system [2].

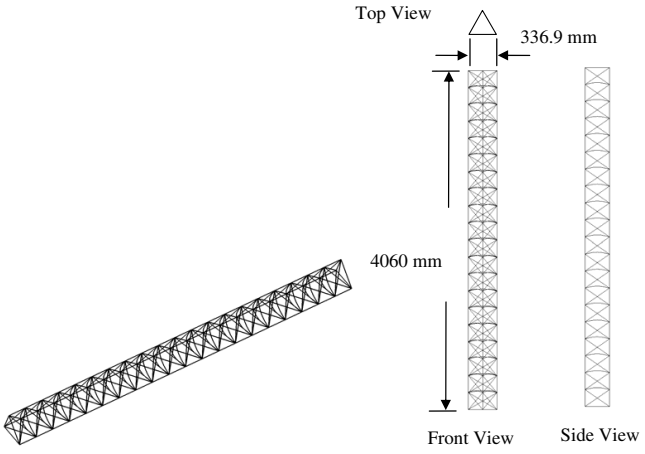

a) Assembled triangular lattice structure **b) Different views**

Fig. 2 Dimensions of the assembled triangular lattice structure.

not be the actual assembly process used by a manufacturer, it is expected that the prestress state of the beam assembled using the proposed process is the same as that in a corresponding beam produced by a manufacturer because both beams have the same geometry and all their components are stressed elastically. To clearly illustrate the proposed assembly process, a two-dimensional (2-D) lattice panel, shown in Fig. 3a, is used to describe the assembly steps in detail. The 2-D panel represents one side of a triangular lattice beam. The longerons are continuous rods. The top and bottom of the longerons are rigidly connected to other structural components, such as end plates or stiff battens. The assembly sequence for the 2-D lattice panel shown in Fig. 3 includes three steps.

The first assembly step is shown in Fig. 3b. Note that the battens are straight. The length of a straight batten is $w + \delta w = 346$ mm, which is longer than the design width $w = 341$ mm of the panel. The shortening δw depends upon the curvature of the assembled batten. In this study, δw is approximately 1.4% of the width of the panel. The straight battens and the longerons are joined together with pinned connectors. The top and bottom of the longerons are not connected to other stiff structural components in this step. Cables are used as diagonals and are linked from the top to the bottom on the longerons through the pulleys at the batten-longeron joints. The upper ends of the two cables are constrained to the top of the longerons, and a tension force is applied to the lower ends of the cables.

The second assembly step is shown in Fig. 3c. A small transverse force, shown as a small arrow, was applied at the midpoint of each batten to cause the battens to bow, while the two longerons were pushed toward each other until the distance between the longerons matched the design width $w = 341$ mm. Once the battens began to bow, the transverse force was gradually reduced to zero. In this step, the tension forces in the cables were kept constant.

The third assembly step is shown in Fig. 3d. The top and the bottom of the longerons were attached to other stiff structural components, and the lower ends of the cables were fixed to the longerons. Finally, the transverse longeron forces were released, and some small adjustments of the cable tension were performed to correct minor width changes needed to ensure the straightness of the longerons. Note that after assembly, the lattice panel was in its equilibrium state with the diagonals tensioned to maintain the shape of the curved battens.

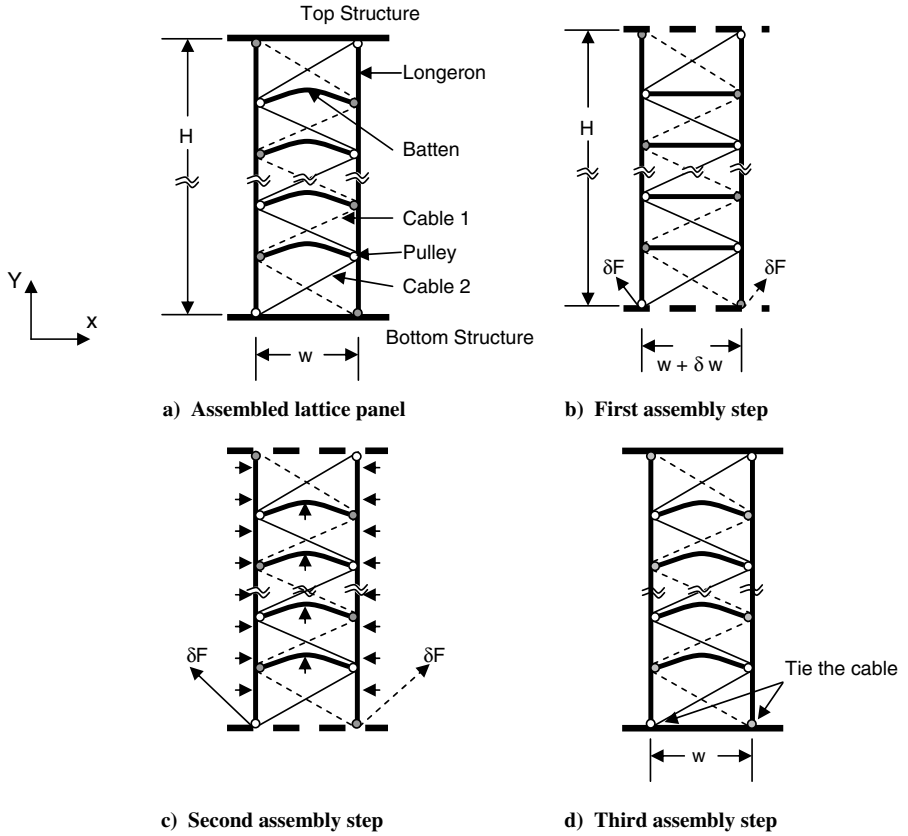

a) Assembled lattice panel **b) First assembly step**

c) Second assembly step **d) Third assembly step**

Fig. 3 Lattice-panel assembly procedure.

Table 1 Material properties

Component name	Young's modulus E, N/mm^2
Longeron	190.0×10^3
Diagonal	120.0×10^3
Batten	200.0×10^3

The assembly process of the 3-D triangular lattice beam shown in Fig. 2a is very similar to that of the 2-D lattice panel, except that in the second step, the three longerons of the 3-D lattice beam were pushed toward the centroid of the triangle. For brevity, the assembly process of the 3-D lattice beam is not presented in this paper.

To be able to predict the assembly induced prestresses in an assembled lattice beam with curved battens, such as the one shown in Fig. 2a, a technique for accurately modeling the assembly process was developed and is presented in this section. To clearly present the modeling techniques, the assembly process of the 2-D lattice panel shown in Fig. 3 was simulated with the ABAQUS FE code and a special user-defined cable-pulley element (see the Appendix for details). The material properties of the panel are presented in Table 1. To adequately model the deformed shapes, each longeron section between two battens was modeled with five beam elements and each batten was modeled with six beam elements. The pinned connections between the longerons and the battens were modeled with multipoint constraints (MPCs) that constrain the three translational displacements to be the same and allow the rotations to be free. The pinned connectors and pulleys were collocated at the batten-longeron joints, shown as circles in Fig. 3. The arrangement of the cable-pulley elements for the assembled 2-D lattice panel is shown in Fig. 4a. A typical cable-pulley element shown in Fig. 4a contains two end nodes (nodes A and C indicated by "**x**" marks) of the cable and one node at the pulley (node B indicated by a solid circle). The first (topmost) cable-pulley element of each cable was tied to the top of the longeron. The cable-pulley element at the bottom has a free end. In the assembly process, a tension force was applied to the free end of the cable to keep it taut. The ABAQUS finite element simulation of the lattice-beam assembly process is divided into three steps.

The first step models the assembly process shown in Fig. 3b. A finite element model was created and all the lattice components were connected together except that the top and bottom structures were not included. In the present models, the straight battens were attached to the longerons using pinned connectors that do not transmit bending moments between the battens and longerons. All 6 degrees of freedom (DOFs) of the longeron elements were constrained, and a small tension force (0.01 N) was applied at the free end of the last cable element of each of the two cables. To get the nonlinear analysis procedure started, the "STABILIZE" option of ABAQUS was used to eliminate the numerical singularities by adding a small artificial viscous force to the model. This artificial force was later removed by a dummy analysis step in which STABILIZE is set to zero.

The second step models the assembly process shown in Fig. 3c. A small transverse force (5 N) was applied at the center of each batten at the beginning of the step. During this step, each of the two longerons was moved toward each other in the x direction by 2.5 mm while the other five DOFs of the longeron nodes were fixed. The transverse force at the center of each batten is gradually removed while the tension force in the cable was kept constant.

The third step models the assembly process shown in Fig. 3d. In this step, the top and bottom structural components with design sizes were added and connected to the longerons. The free ends of the cables were fixed at the bottom of the longerons. Finally, all of the constraints on the longerons in the previous steps were released, and the structure reached an equilibrium state.

The equilibrium shape of the lattice was examined. If the midsection of the structure had any minor deviation from the design width after the release of the longeron constraints, this deviation was corrected by adjusting the tension forces of the cables to ensure the straightness of the longerons. For the assembled model shown in Fig. 3a, the vertical displacement at the midpoint of the batten is about 26 mm, and the tension force in the cable is about 3.6 N.

The simulation of the assembly process for the 3-D triangular lattice beam is similar to that of the 2-D lattice panel except that in the second simulation step, the three longerons of the 3-D lattice structure were moved toward the centroid of the triangle by 2.5 mm. Because of the similarity, the ABAQUS simulation of the assembly process of the 3-D lattice beam is not presented in this paper.

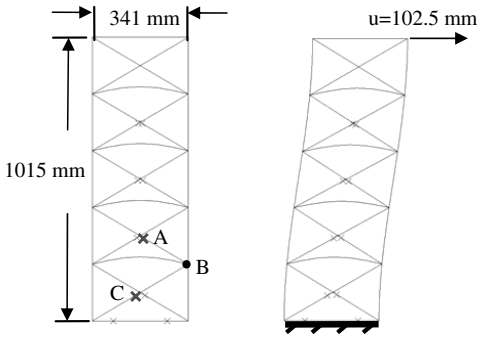

a) Initial shape **b) Deformed shape**

Fig. 4 Lattice panel with curved battens and tensioned continuous diagonals (BCDC model).

Finite Element Models of the Assembled Lattice Structures

Three types of FE models were developed to investigate the effects of batten curvatures, assembly induced prestresses, and diagonal-cable constraints on the load-carrying capabilities of the lattice structures, including the lattice panel and the lattice beam. The first type of FE model is named the BCDC model, in which the battens are curved and the diagonals are continuous and tensioned. The corresponding 2-D assembled lattice-panel model shown in Fig. 4 contains compressed curved battens, nearly straight longerons, and tensioned continuous diagonals. Note that the assembly induced stresses were included in the model. The batten-longeron joint has a low-friction rail for the diagonal cable that can be approximated by a frictionless pulley. Therefore, the continuous diagonals were modeled with frictionless cable-pulley elements.

The second type of FE model used in the present study is called the BCDD model. In this model, the battens are curved and the diagonals are discontinuous. The BCDD model has the same geometry as the assembled BCDC model, but the diagonal cables are fixed (glued) at every batten-longeron joint. The model does not have cable-pulley elements. The diagonals were modeled by truss elements with no compression modulus. Because the diagonal cables of typical deployable lattice beams are fixed at the joints, this type of the model is considered to be the most accurate one for modeling lattice beams. The BCDD model contains the assembly induced prestresses, but they can be removed for studying the prestress effects on the loading responses of the lattice beam.

Note that the cable-pulley element can also be used to model a diagonal-cable constraint failure. For example, the BCDC model can be considered as the BCDD model in which all the diagonal constraints have failed. The unconstrained diagonals, which can slip through the joints, are modeled with cable-pulley elements.

The third type of the FE model considered herein is called the BSDD models, in which battens are straight and diagonals are discontinuous. At the design and development stage, batten curvature information may not be available to structural analysts. Therefore, the battens are often considered to be straight instead of curved and the tension in the diagonals is neglected. The model does not have the assembly induced prestresses. The BSDD model is used as a baseline to determine the effect of the curved battens on the load-carrying capability of a lattice beam. For this model, the assembly process was not simulated, and the length of the battens is the same as the width of the assembled BCDD model. In the BSDD models, the battens were modeled with beam elements, and the diagonals were modeled with truss elements with a negligible compression modulus.

Table 2 Cross-sectional dimensions

Component name	Cross-sectional shape	
	Circular (radius)	Rectangular
Longeron	1.23 mm	——
Diagonal	0.37 mm	——
Batten	——	1.3 mm × 1.5 mm

Loading Responses of Cantilevered Lattice structures

For the 2-D lattice panel and the 3-D triangular lattice beam considered herein, all three types of FE models described previously were created and subjected to a transverse displacement with a cantilever boundary condition. Geometrically nonlinear analyses were performed until the converged solutions were no longer obtained. The deflections and deformation patterns of all types of models are presented subsequently.

Loading Responses of 2-D Lattice-Panel Models

The dimensions of the assembled 2-D panel are shown in Fig. 4 and Table 2. The panel is composed of five bays. The dimensions of all the assembled models are the same except that the BSDD model has straight battens. The BCDC, BCDD, and BSDD lattice-panel models were subjected to a transverse displacement (u) at the right top corner and a clamped boundary condition at the lower end, as shown in Figs. 4–6. Note that the nonlinear analysis solution for the models cannot be converged when the applied u displacement is beyond what is shown in the corresponding deformed plot. The deformed shapes of the three lattice-panel models are also shown in Figs. 4–6. The deformed shape of the BCDC model shown in Fig. 4 is dominated by shear deformation of the bays. The top of the structure remains nearly parallel to the bottom. The applied transverse displacement induces different tensions in the two cables. However, the tension in each of the two cables remains constant along their length due to the use of cable-pulley elements. The curvature of the battens increases a little with the deformation. No local buckling of the longerons is observed.

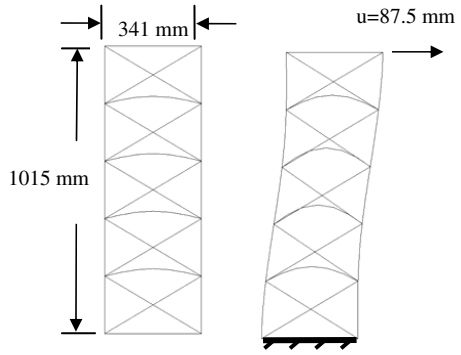

Fig. 5 Lattice panel with curved battens and tensioned discontinuous diagonals (BCDD model).

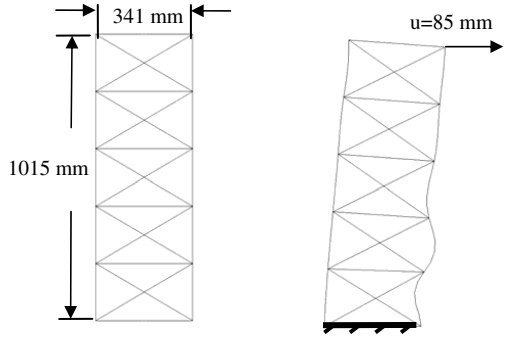

Fig. 6 Lattice panel with straight battens and discontinuous diagonals (BSDD model).

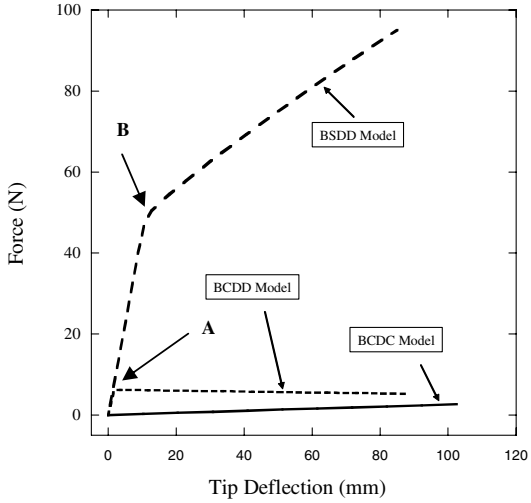

Fig. 7 Transverse force versus tip deflection of cantilevered lattice panels.

The deformed shape of the BCDD model is shown in Fig. 5. The deformation is also dominated by shear deformation and the top remains nearly parallel to the bottom. No local buckling of the longerons occurs. However, the batten curvatures in Fig. 5b are significantly greater than those shown in Fig. 5a. Following the batten deformations, the two longerons moved closer to reduce the midsection width of the lattice panel.

The deformed shape of the BSDD model is shown in Fig. 6. The bending deformation induces a local buckling of the longeron at the compression side. The straight battens are perpendicular to the unbuckled longeron (left side) indicating that there is little shear deformation of each bay. Therefore, the straight battens and discontinuous diagonals can substantially increase the shear stiffness.

The load versus tip-deflection curves for the three lattice-panel models are shown in Fig. 7. The transverse load-carrying capability of the BCDC model is very low. The deformation of the BCDC model is mainly from shear deformation. In pure shear deformation, a rectangular lattice bay becomes a parallelogram, where one diagonal is stretched and the other is shortened. The stretched diagonal in a lattice bay develops a tension force to resist the shear deformation. Because the cable diagonal cannot carry compression loads, only the tensioned diagonals contribute to shear stiffness of the structure. By using continuous diagonals, the cable can slip through the pulley into the adjacent bays and the tension force cannot be developed. Therefore, the use of continuous diagonals in the BCDC model results in little resistance to shear deformations.

The BCDD model can carry a slightly higher load than the BCDC model, as shown in Fig. 7. After the maximum load (point A) is reached, the load-carrying capability of the BCDD model is reduced. The reduction of the load-carrying capability is due to the increase of the batten curvature and the decrease of the panel width as shown in Fig. 5.

The BSDD model with straight battens has the highest load-carrying capability. The discontinuous diagonals reduce the shear deformations of the BSDD model because each bay in the model has its own tension diagonals. The straight battens provide stiffer supports to the longerons to increase the longeron's critical buckling load (point B), because the straight battens have higher axial stiffness than the curved battens. The tip deflection is dominated by the bending deformation because the bays do not deform in shear. The bending moment of the structure induces compression loads in a longeron to cause local buckling. After the longeron buckles, the bending rigidity of the structure is reduced, but the loading capability is continuously increased, as shown in Fig. 7.

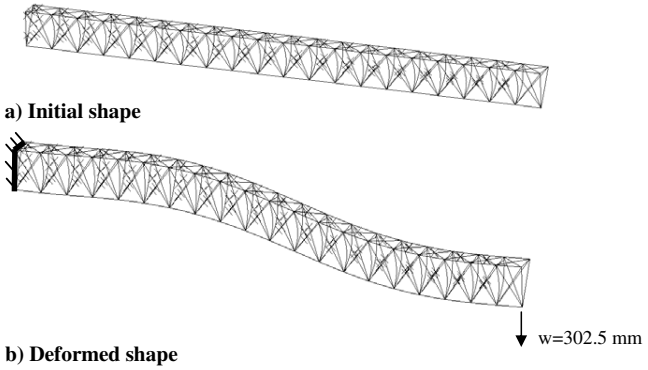

Fig. 8 Triangular lattice beam with curved battens and tensioned continuous diagonals (BCDC model).

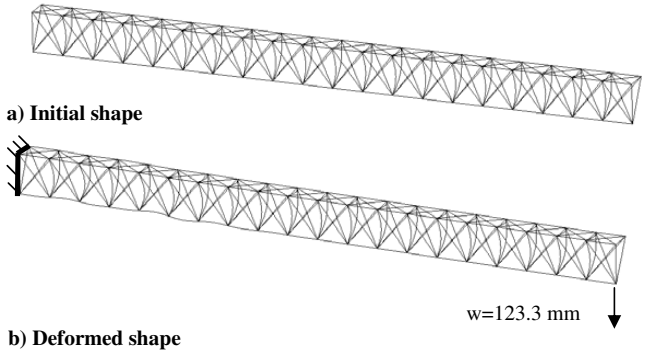

Fig. 9 Triangular lattice beam with curved battens and tensioned discontinuous diagonals (BCDD model).

Loading Responses of 3-D Triangular Lattice-Beam Models

The dimensions of the assembled 3-D triangular lattice beam that has 20 bays are shown in Fig. 2b and Table 2. Corresponding BCDC, BCDD, and BSDD models of this triangular lattice beam were developed and analyzed. These models were subjected to an applied transverse tip displacement at one end of the structure while the other end was fixed. The mesh densities are the same as the 2-D models.

The deformed shape of the BCDC model (curved battens and continuous diagonals) is shown in Fig. 8b for a tip deflection of 302.5 mm. The battens of the BCDC model remain nearly parallel to each other during deformation. This aspect indicates that the deformation is dominated by the shear deformation that is caused by the use of the continuous diagonals, as exhibited by the corresponding 2-D model.

The deformed shape of the BCDD model (curved battens and discontinuous diagonals) is shown in Fig. 9b for a significantly smaller tip displacement of 123.3 mm. The nonlinear analysis could not be converged when the applied displacement is beyond 123.3 mm. The compressed lower longeron buckles near the fixed end. The dominant deformation mode of the structure is bending, which is different from the 2-D BCDD model, where the main deformation mode of the 2-D model is shear. The lower longeron of the triangular lattice beam is supported by two battens at each connection point. The bay-shape changes and the shear deformations were reduced due to the stronger support at the connection points. An additional analysis of the 2-D BCDD model was conducted to confirm this hypothesis. In the analysis, the modulus of the battens was doubled to provide stronger support to the longeron. Indeed, the lattice panel deforms in bending with local buckling similar to those of the 3-D model.

The deformed shape of the BSDD model (straight battens and discontinuous diagonals) with a tip deflection of 354.7 mm is shown in Fig. 10b. The dominant deformation mode of the structure is bending. The compressed lower longeron buckles near the fixed end of the lattice structure. Because of a greater tip displacement applied,

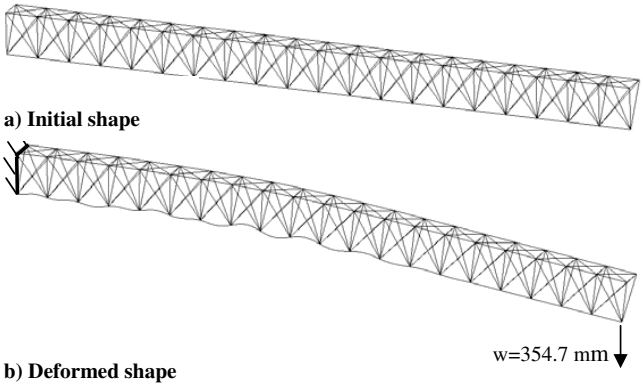

Fig. 10 Triangular lattice beam with straight battens and discontinuous diagonals (BSDD model).

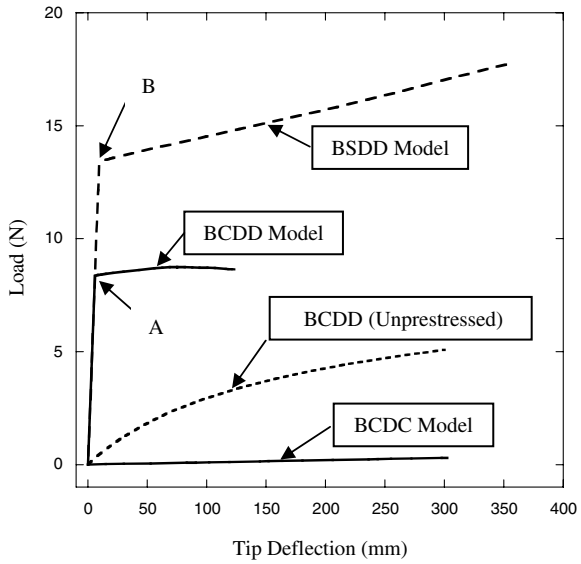

Fig. 11 Transverse force versus tip deflection of cantilevered triangular lattice-beam models.

the extent of the buckle is much more pronounced than that of the BCDD model.

The load-deflection curves of all models are shown in Fig. 11. The BCDC model has very little capability for carrying the transverse shear load because the cable diagonals are continuous from bay to bay, which is similar to the 2-D BCDC model. The BCDD model deforms in bending because the cable diagonals are constrained at every batten-longeron joint, resulting in a higher shear stiffness associated with each bay, as shown in Fig. 9b. In addition, the load-carrying capability to the BCDD model is much greater than the BCDC model. The local buckling of the compressed lower longeron occurs at point A in Fig. 11. After the local buckling, the bending rigidity is greatly reduced, and the structure can carry little additional load. Note that the flat slope of the load-deflection curve that corresponds to a buckled configuration indicates very little postbuckling load-carrying capability. Numerical difficulties are encountered after the tip deflection reaches about 120 mm, and converged solutions cannot be obtained.

To investigate the effects of prestresses on the loading responses of the BCDD model, an additional 3-D BCDD (unprestressed) model was created. The BCDD (unprestressed) model is identical to the assembled BCDD model except the battens were manufactured to be curved instead of being forced to be curved elastically in the assembly process. The BCDD (unprestressed) model has no tension stresses in the diagonals and no axial compression stresses in the curved battens. Under the same loading and boundary conditions, the load-deflection curve of the BCDD (unprestressed) model was

obtained and plotted in Fig. 11. The load-deflection curve shows that the unprestressed BCDD model exhibits a monotonically increasing nonlinear response. The overall bending stiffness of the unprestressed BCDD model is much less than that of the prestressed BCDD model. The deformed shape of the unprestressed BCDD model was also examined and it was found that no local buckling occurred. These results indicate that the batten prestress significantly affects the bending stiffness. In particular, the bending stiffness is a highly nonlinear function of the batten deformation and the corresponding relative distance between the longerons.

The buckling load (point B) and the postbuckling stiffness of the BSDD model are much greater than those of the BCDD model, as shown in Fig. 11. This increased buckling strength is due to the greater support provided to the longerons by the straight battens, in contrast to that provided by the curved battens. The model with straight battens has the highest load-carrying capability. After buckling of the lower longeron, the slope of the load-deflection curve is reduced. The slope change is due to the fact that the buckled longeron has a smaller effective axial stiffness, and some portion of the longeron axial load may redistribute to other members within the model. However, the load-carrying capability of the BSDD model continues to increase. Because the BCDD model includes all the structural details of a typical deployable triangular lattice beam, it is the most physically accurate model presented herein. Thus, using the conventional engineering BSDD model may result in an overprediction of the load-carrying capability of an actual lattice-beam design.

The results presented in Fig. 11 are also useful for assessing the effects of failures or defects in lattice beams discussed herein. As mentioned previously, the BCDD model becomes a BCDC model when all diagonals are not fixed to the batten-longeron joints and are allowed to slip through the joints. Such a loss of constraints can be caused by glue failures. By examining the load-deflection curves of both the BCDD and BCDC models in Fig. 11, one can conclude that this type of failure or manufacturing defect can have a detrimental effect on the load-carrying capability of the triangular lattice beam. The BCDC model, which has little load-carrying capability, represents an extreme failure case of the BCDD model. Other failure cases, such as the failure of a few diagonal constraints in the BCDD model, can also be investigated by using the same modeling techniques presented herein.

Concluding Remarks

An integrated modeling technique for the analysis of triangular lattice beams with curved battens has been presented. This modeling technique was used to simulate a manufacturing assembly process for a lattice beam and to account for the assembly induced prestresses and curvature of the battens in the subsequent loading response analysis. To simulate the assembly process, a cable-pulley element was implemented in a general-purpose finite element analysis code as a user-defined element and geometrically nonlinear finite element analyses were performed.

Following the assembly simulation, the finite element model of the assembled lattice beam in a prestress state was converted to several finite element models for the loading response analyses. The analysis results were used to evaluate the effects of diagonal constraints, batten curvatures, and assembly induced prestresses on the load-carrying capability of a current lattice-beam design. The first model is the assembled lattice-beam model that consists of curved battens and continuous cable diagonals. The second model is the same as the first model except that the cable diagonals are discontinuous because they are constrained (glued) at the batten-diagonal joints. Because the second model has all the features such as curved battens, discrete cable diagonals, and tensional diagonals of a current deployable triangular lattice-beam design, it is the most accurate model for representing an actual deployable lattice beam. The third model is obtained from the second model by replacing its curved battens with straight battens. Loading response analyses were performed for these lattice models cantilevered at one end and subjected to a transverse-shear tip load at the other end. To investigate the effect of the prestress state on the load-carrying capability of a lattice beam, the second model with all the assembly induced prestresses removed was analyzed.

The results from the first and second models show that using discontinuous instead of continuous diagonals produces a higher transverse shear stiffness. The first model, with continuous diagonals, exhibits large shear deformations and has a very low load-carrying capability.

The results from the second and third models show that using straight battens produces a higher bending stiffness than using curved battens. For all the models analyzed, the model with straight battens has the highest load-carrying capability. Because the current deployable triangular lattice beams contain curved battens, using models with straight battens can result in an overprediction of their load-carrying capabilities.

Finally, this study found that the assembly induced prestresses can significantly affect the load-carrying capability and the deformation mode of a lattice beam. Without including the prestress state of a lattice beam in the loading response predictions, its loading capability could be underpredicted. For accurately predicting the prestress state, the assembly process of a lattice beam needs be carefully simulated.

Appendix: Cable-Pulley Element

The cable and pulley mechanism is commonly used in mechanical and structural systems. A cable-pulley element was implemented in ABAQUS based on [7]. Figure A1a shows the configuration of a cable with ends N_1 and N_2 passing through a pulley N_3. Figure A1b shows the internal force of the element. To model large displacements of the cable and the pulley, a geometrically nonlinear finite element method is used.

The assumptions used for the cable-pulley element are the following:

1) The cable is perfectly flexible and can only carry tension force.

2) The radius of the pulley is zero.

3) The pulley is frictionless. The tension force in the cable segments is constant ($|\mathbf{F}_1| = |\mathbf{F}_2|$). The equilibrium condition of the element is $\mathbf{F}_3 = -(\mathbf{F}_1 + \mathbf{F}_2)$.

4) Thermal effects are negligible.

5) The weight of the cable is negligible (the sag effect is not considered).

6) The cable-pulley element can be used to model large displacements for both the cable and the pulley.

7) The strain of the cable is small (Poisson's effect of the cable is not considered).

With the aforementioned assumptions, the cable-pulley element can be idealized as shown in Fig. A1b. The two strands N_1N_3 and N_2N_3 remain rectilinear. The length vectors representing the two strands can be written as

$$\mathbf{L}_1 = \mathbf{X}_1 + \mathbf{U}_1 - (\mathbf{X}_3 + \mathbf{U}_3) \qquad \mathbf{L}_2 = \mathbf{X}_2 + \mathbf{U}_2 - (\mathbf{X}_3 + \mathbf{U}_3) \tag{A1}$$

$$|L_1| = \sqrt{\mathbf{L}_1^T \mathbf{L}_1}, \qquad |L_2| = \sqrt{\mathbf{L}_2^T \mathbf{L}_2} \tag{A2}$$

$$\mathbf{l}_1 = \mathbf{L}_1/|L_1|, \qquad \mathbf{l}_2 = \mathbf{L}_2/|L_2| \tag{A3}$$

where $\mathbf{X}_i$, $\mathbf{U}_i$ are the coordinates and the displacement vectors of the ith node, respectively. $\mathbf{L}_i$ and $\mathbf{l}_i$ are the vector and the unit vector of the ith cable strand, respectively. $|L_i|$ is the length of the ith cable strand.

The cable is assumed to be linear elastic and the constitutive relation between the tension force N and cable strain ε can be expressed as

$$N = \begin{cases} EA\varepsilon & \varepsilon \geq 0 \\ 0 & \varepsilon < 0 \end{cases} \tag{A4}$$

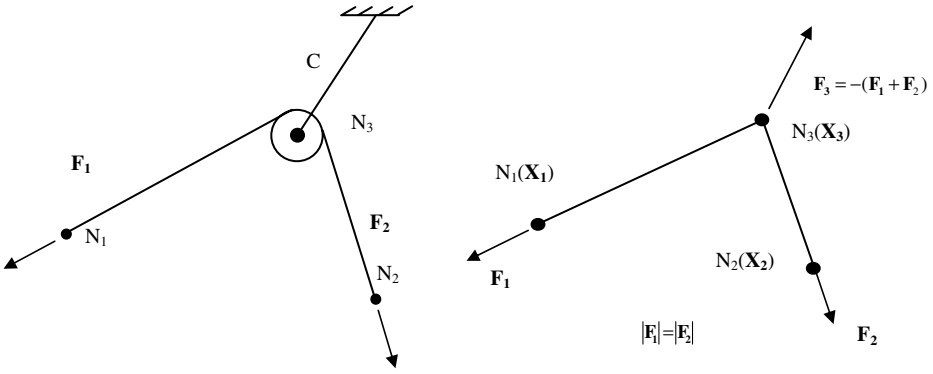

a) Actual configuration **b) Cable-pulley element**

Fig. A1 Cable element used to model a cable passing through a pulley.

where E and A are the modulus and area of the cross section of the cable, respectively. The strain ε must remain small, so that the cross-sectional area, A, of the cable is unchanged. The strain ε is defined as

$$\varepsilon = (|L_1| + |L_2| - |L|_0)/|L|_0 \tag{A5}$$

where $|L|_0$ is the total unstrained length of the cable $|L|_0 = |L_1|_0 + |L_2|_0$.

The points N_1, N_2, and N_3 of Fig. A1b are referred to as nodes of the element, and the third node, N_3, is at the location of the pulley. The internal forces are the forces that must be exerted on the nodes to keep it in its equilibrium configuration, as shown in Fig. A1b. These forces are defined as

$$\mathbf{F}_1 = N \cdot \mathbf{l}_1, \qquad \mathbf{F}_2 = N \cdot \mathbf{l}_2, \qquad \mathbf{F}_3 = -(\mathbf{F}_1 + \mathbf{F}_2) \tag{A6}$$

The incremental nodal displacements and the incremental internal forces of the nonlinear cable element are defined as

$$\delta\mathbf{U} = \begin{Bmatrix} \delta\mathbf{U}_1 \\ \delta\mathbf{U}_2 \\ \delta\mathbf{U}_3 \end{Bmatrix}, \qquad \delta\mathbf{F} = \begin{Bmatrix} \delta\mathbf{F}_1 \\ \delta\mathbf{F}_2 \\ \delta\mathbf{F}_3 \end{Bmatrix} \tag{A7}$$

and they are related as

$$\delta\mathbf{F} = \mathbf{K} \cdot \delta\mathbf{U} \tag{A8}$$

where $\mathbf{K}$ is the tangent stiffness matrix and $\delta\mathbf{F}$ can be calculated by [9]

$$\delta\mathbf{F} = \lim_{\eta \to 0} \frac{d}{d\eta} \mathbf{F}(\mathbf{U} + \eta \cdot \delta\mathbf{U}) \tag{A9}$$

The final expression of $\mathbf{K}$ is

$$\mathbf{K} = \begin{bmatrix} \mathbf{K}_{11} & \mathbf{K}_{12} & -(\mathbf{K}_{11} + \mathbf{K}_{12}) \\ \mathbf{K}_{12}^T & \mathbf{K}_{22} & -(\mathbf{K}_{22} + \mathbf{K}_{12}^T) \\ -(\mathbf{K}_{11} + \mathbf{K}_{12}^T) & -(\mathbf{K}_{22} + \mathbf{K}_{12}) & -(\mathbf{K}_{13} + \mathbf{K}_{23}) \end{bmatrix} \tag{A10}$$

where

$$\mathbf{K}_{11} = \left(\frac{EA}{|L|_0} - \frac{N}{|L_1|}\right)\mathbf{l}_1 \cdot \mathbf{l}_1^T + \frac{N}{|L_1|}\mathbf{I}_3$$
$$\mathbf{K}_{22} = \left(\frac{EA}{|L|_0} - \frac{N}{|L_2|}\right)\mathbf{l}_2 \cdot \mathbf{l}_2^T + \frac{N}{|L_2|}\mathbf{I}_3 \qquad \mathbf{K}_{12} = \frac{EA}{|L|_0}\mathbf{l}_1\mathbf{l}_2^T \tag{A11}$$

where $\mathbf{I}_3$ is a 3×3 identity matrix.

Acknowledgements

The work presented in this paper was funded in part by the In-Space Propulsion Technology Program, which is managed by NASA's Science Mission Directorate in Washington, D.C., and implemented by the In-Space Propulsion Technology Office at Marshall Space Flight Center in Huntsville, AL. The authors would like to gratefully acknowledge the associate editor and reviewers for their valuable comments.

References

[1] Murphy, D., Trautt, T., McEachen, M., Messner, D., Laue, G., and Gierow, P., "Progress and Plans for System Demonstration of a Scalable Square Solar Sail," *Advances in the Astronautical Sciences*, Vol. 119, Pt. 1, 2005, pp. 51–68.

[2] Murphy, D. M., Macy, B. D., and Gaspar, J. L., "Demonstration of a 10-m Solar Sail System," *Proceedings of the 45th AIAA/ASME/ASCE/AHS/ASC Structures, Structural Dynamics & Materials Conference*, AIAA, Reston, VA, 19–22 April 2004; also AIAA Paper 2004-1576.

[3] Crawford, R. F., and Hedgepeth, J. M., "Effects of Initial Waviness on the Strength and Design of Built-up Structures," *AIAA Journal*, Vol. 13, No. 5, 1975, pp. 672–675.

[4] Mikulas, M. M., "Structural Efficiency of Long, Lightly-Loaded Truss and Isogrid Columns for Space Applications," NASA TM 78687, July 1978.

[5] Crawford, R. F., and Benton, M. D., "Strength of Initially Wavy Lattice Columns," *AIAA Journal*, Vol. 18, No. 5, 1980, pp. 581–584.

[6] Noor, A. K., "Continuum Modeling for Repetitive Lattice Structures," *Applied Mechanics Reviews*, Vol. 41, No. 7, 1998, pp. 285–296.

[7] Aufaure, M., "A Finite Element of Cable Passing through a Pulley," *Computers and Structures*, Vol. 46, No. 5, 1993, pp. 807–812.

[8] ABAQUS Analysis User's Manual, Ver. 6.5, ABAQUS Inc., Providence, RI, 2004.

[9] Cardona, A., and Geradin, M., "A Beam Finite Element Nonlinear Theory with Finite Rotations," *International Journal for Numerical Methods in Engineering*, Vol. 26, No. 11, 1988, pp. 2403–2438.

M. Nemeth
Associate Editor